Catalysis Science & Technology

Accepted Manuscript

ROYAL SOCIETY OF CHEMISTRY

www.rsc.org/catalysis

Table of Content

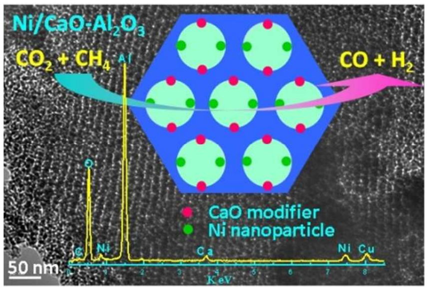

Significant roles of mesostructure and basic modifier in improving the catalytic performance of dry reforming were investigated.

Significant roles of mesostructure and basic modifier for ordered mesoporous Ni/CaO-Al_2O_3 catalyst towards CO_2 reforming of CH_4

Leilei Xu [a, c]*, Zhichao Miao [a, b], Huanling Song [a], Wei Chen [c]*, Lingjun Chou [a]*

[a] State Key Laboratory for Oxo Synthesis and Selective Oxidation, Lanzhou Institute of Chemical Physics, Chinese Academy of Sciences, Lanzhou 730000, P.R. China.

[b] University of Chinese Academy of Sciences, Beijing 100049, P.R. China.

[c] Department of Chemistry, National University of Singapore, 3 Science Drive 3, 117543 Singapore

*Corresponding author,

Leilei Xu, Tel.: +65 96382289; E-mail: chmxul@nus.edu.sg, and leileixu88@gmail.com

Wei Chen, Tel.: +65 6516 2921; E-mail: phycw@nus.edu.sg, and chmcw@nus.edu.sg

Lingjun Chou, Tel.: +86 931 4968066; Fax: +86 931 4968129; E-mail: ljchou@licp.cas.cn

Abstract

Ordered mesoporous CaO-Al_2O_3 composite oxide had been designed and prepared via improved evaporation induced self-assemble strategy (EISA). The resultant material was utilized as the support of Ni based catalyst for CO_2 reforming of CH_4. In order to study the roles of ordered mesopore and basic modifier in promoting the catalytic properties toward CO_2 reforming of CH_4 reaction, non-mesoporous CaO-Al_2O_3 without ordered mesostructure and ordered mesoporous Al_2O_3 without basic modifier were also synthesized, respectively. It was found that both the ordered mesostructure and CaO basic modifier showed significant effects in promoting catalytic activity, stability and suppressing the carbon deposition during their 100 h long term stability tests. Compared with traditional supported catalyst, the confinement effect of the mesoporous catalysts could effectively inhibit the thermal sintering of the Ni particles. Furthermore, the sorts of the coke species over the spent catalysts and the mechanism of catalyst deactivation were also carefully investigated. Therefore, the present ordered mesoporous CaO-Al_2O_3 composite oxide will be a potential carrier for Ni based catalysts for CO_2 reforming of CH_4 and even other reactions.

Keywords: ordered mesoporous; confinement effect; CaO-Al_2O_3; basic modifier; CO_2

reforming; CH_4

1. Introduction

In the past decades, the industry around the worldwide has enjoyed rapid development, which has been consumed huge amounts of fossil fuels, such as petroleum, coal, etc. As a result, a large number of carbon dioxide, known as the cheapest carbon source, is emitted into the atmosphere, which further gives rise to the global greenhouse effect [1-4]. Besides, the proved reserves of the natural gas (methane) among the worldwide have been increasing in recent years. At the same time, methane, another greenhouse gas, is commonly recognized as one of the most stable organic compounds. Therefore, how to efficiently utilize these two problematic C1 gases has been attracted a considerable interest [5, 6]. Here, the present carbon dioxide reforming of methane (CRM) catalytic process provides a promising route to convert these gases into high value-added synthesis gas with low H_2/CO ratio (1/1 or less), which is desirable for many processes, such as oxo synthesis, hydroformylation, and so on [7, 8]. Furthermore, this catalytic process is an intensely endothermic reaction. Thus, if it is driven by green energies, such as solar energy, wind energy, tidal energy, geothermal energy, etc, these carbon-free energies can be stored as chemical energy in the form of H_2 and CO, which can be easily transported to remote energy shorted areas through pipeline [9, 10]. However, up to now, no large scale industrial technology for CRM process has been developed yet. The main reason for this is the rapid deactivation of the catalyst, especially for non-noble catalysts, such as Ni, Co, and so on.

Ni based catalyst are one of the most important catalysts for CRM reaction due to its low cost and high activity. However, under reforming conditions (usually at high temperature), Ni catalysts are prone to form Ni clusters and deposited carbon, which will finally lead to quick catalyst deactivation [4, 11]. Therefore, effectively suppressing the thermal sintering of metallic Ni particles and the formation of surface coke are the current research focuses as well as big challenges. Generally, the thermal sintering of the metallic Ni nanoparticles is effectively controlled by confining the Ni in some well-defined structures, such as spinel [12-14], perovskite [15-19], solid solution [20-22], hexaaluminate [23, 24], etc. But their greatest drawback is that their structural properties, such as surface areas, pore volumes, are not very satisfying. As a result, they will not provide gaseous reactants with sufficient Ni active centers. Besides, in order to minimize the carbon deposition, researchers usually regulate the surface structure and acidity of the catalyst. Specifically, by controlling the size of metallic Ni ensembles and surface property of the support, it is possible to command the coke formation. Pioneer studies indicated that carbon deposition occurs more easily on larger nickel clusters than smaller counterparts [25, 26]. In other words, Ni clusters with smaller size have a better ability to inhibit coke. Furthermore, coke formation is favored by acidic supports [27]. It has been proved that the carbon deposition can be attenuated or suppressed when the metal is supported on metal oxides with strong Lewis basicity [28, 29]. The reason for this derives that the increase of the Lewis basicity of the support enhances the ability of the catalyst to chemisorb CO_2 in CRM reaction. As a result, the adsorbed CO_2 will take part in the process of coke elimination ($C + CO_2 \rightarrow 2CO$), finally resulting in the reduction of coke formation.

In our former works, we had designed a series of ordered mesoporous $NiO\text{-}Al_2O_3$, $NiO\text{-}MgO\text{-}Al_2O_3$, and $NiO\text{-}CaO\text{-}Al_2O_3$ composite oxides via one-pot synthesis strategy and directly used them as the catalysts for CRM reaction [30-32]. Compared with the traditional supported Ni catalysts, these mesoporous catalysts indeed performed enhanced catalytic activities and stabilities. The reasons ought to be attributed to the following aspects. Specifically, the good structural properties of the mesoporous materials were able to provide sufficient Ni active sites for the reactants; the mesoporous framework could confine the Ni active sites within nanometer size due to the unique advantage of the one-pot synthesis method. Therefore, previous research experiences inspired us if we can design a sort of catalytic carrier with ordered mesostructure and basic modifier, which might be the promising support of Ni based catalyst. It was supposed that the ordered mesoporous channels might be able to limit the thermal growth of the Ni nanoparticles via the confinement effect of mesoporous channel according to pioneer literatures [29, 33]. Besides, the presence of basic modifier would improve the catalytic performance via enhancing the chemisorption of CO_2.

Herein, ordered mesoporous $CaO\text{-}Al_2O_3$ composite oxide was designed and synthesized by improved evaporation induced self-assembly method. The obtained material with excellent structural property and high thermal stability was utilized as the carrier for Ni based catalysts for CRM reaction. The roles of mesostructure and CaO basic modifier in promoting the catalytic performance, especially suppressing coke, for CRM were carefully studied. The possible mechanism for deactivation of Ni based catalyst was also investigated.

2. Experimental

2.1. Synthesis of catalyst carriers

Ordered mesoporous CaO-Al_2O_3 composite oxide was synthesized via improved evaporation induced self-assemble (EISA) strategy based on the pioneer literature [34]. In a typical synthesis procedure, approximately 1.0 g $(EO)_{20}(PO)_{70}(EO)_{20}$ triblock copolymer (Pluronic P123, M_n = 5800, Sigma-Aldrich) was dissolved in 20.0 mL absolute ethanol with vigorous stirring. Then, 1.6 mL of 67.0 wt% nitric acid, 10 mmol aluminum isopropoxide (98+%, Sigma-Aldrich), and 0.3 mmol $Ca(NO_3)_2{\cdot}4H_2O$ (Sinopharm Chemical Reagent Co., Ltd) were added in sequence. After vigorously stirring for at least 5h at room temperature, the transparent homogeneous sol was transferred to a Perish dish. Then put the dish into a drying oven under desired temperature and humidity (temperature: 60 ^oC, relative humidity: 50%) to undergo solvent evaporation for 48 h. A white xerogel was obtained after EISA process. Calcination was carried out by slowly increasing temperature from room temperature to 700 ^oC with 1 ^oC/min ramping rate and heating at this temperature for 5 h in air. The final mesoporous materials were labeled in the general form OMA-3Ca, where OMA stood for “ordered mesoporous alumina matrix”, 3 referred to the molar percentage between Ca and Al (3 mol% = $n_{Ca}/n_{Al} \times 100\%$, n_{Al} = 10 mmol, n_{Ca} = 0.3 mmol), respectively.

In order to investigate the effect of the Ca basic modifier, ordered mesoporous alumina (denoted as OMA) without Ca modification was facilely synthesized via EISA strategy according to the literature reported by Yuan etc [34]. Besides, for the purpose of studying the role of uniform mesopore channel, CaO-Al_2O_3 composite oxide without ordered mesoporous structure (denoted as NPA-3Ca, where NPA stood for “non-mesoporous alumina” and the meaning 3 was still same as that of OMA-3Ca) was also prepared. The preparation method of NPA-3Ca was similar to that of OMA-3Ca, just without the addition of Pluronic P123 template.

2.2. Preparation of catalysts

Nickel based catalysts supported on OMA-3Ca, OMA, and NPA-3Ca containing 5 wt% Ni (5 wt% = $m_{Ni}/(m_{Ni} + m_{carrier}) \times 100\%$) were prepared via incipient impregnation method assisted with

3 h ultrasound treatment (shanghai BRANSON SB5200, P = 280 W, ultrasonic frequency = 37 kHz) using $Ni(NO_3)_3.6H_2O$ (Shanghai NO. 2 Reagent Factory, China) as the precursor of nickel. After impregnation, the catalyst precursors were dried in a 60 ^oC drying oven for 24 h. Finally, the catalyst precursors were calcined at 700 ^oC for 5 h. All catalysts obtained were pressed, crushed, and sieved through 20-40 meshes. The obtained catalysts were denoted as 5%Ni/OMA-3Ca, 5%Ni/OMA, and 5%Ni/NPA-3Ca in the following text.

2.3. Catalyst characterization

XRD patterns were recorded by an X'pert Pro multipurpose diffractiometer (PANalytical, Inc.) with Ni-filtered Cu Kα radiation (0.15046 nm). The nitrogen adsorption and desorption isotherms at -196 ^oC were measured using an Autosorb-iQ analyzer (Quantachrome Instruments U.S.). TEM images, selective area electron diffraction (SAED), and energy-dispersive X-ray spectroscopy (EDX) measurements were performed on the FEI F20 (Netherlands) high-resolution transmission electron microscopy under a working voltage of 200 kV. XPS analyses of the catalysts were performed on a Thermo Fisher Scientific K-Alpha spectrometer. H_2 temperature programmed reduction (H_2-TPR) measurements were performed on AMI-100 unit (Zeton-Altamira instrument, U.S.) employing 5 mol % H_2-He as reducing agent and the hydrogen consumption was measured using an AMETEK (LC-D-200 Dycor AMETEK) mass spectrometer. CO_2 temperature programmed desorption (CO_2-TPD) measurements were carried out on the same apparatus as described for H_2-TPR. Thermogravimetric (TG) measurements were carried out on a NETZSCH STA 449F3 thermogravimetric analyzer from room temperature to 900 ^oC with the rate of 10 ^oC/min under air atmosphere.

2.4. Catalytic activity measurements

Catalytic tests were performed at atmospheric pressure (1 atm) in a vertical fixed-bed continuous flow quartz reactor (8 mm, i.d.). The temperature of reaction bed was monitored by a coaxial thermocouple. The flow rate of reactant gas was precisely regulated by mass flow controllers (MT50-4J METRON Instruments). For each test, 100 mg catalyst diluted with 350 mg quartz sand (20-40 meshes) was used in each run. Prior to the reaction, the catalyst was in situ reduced in a mixed flow of H_2 and N_2 (H_2/N_2 = 10/20 mL/min) at 800 ^oC for 120 min. Before introducing in the reaction gases, the catalyst bed was purged with N_2 for half an hour to remove the absorbed hydrogen. Then, the reaction mixture was fed into the reactor. The final products were analyzed on line by the gas chromatograph equipped with TDX-01 packed column. Blank test was also performed prior to regular catalytic experiments and behaved negligible catalytic activity even at temperature as high as 800 ^{o}C. The conversions of the gaseous reactants were calculated based on the carbon balance.

3. Results and discussion

3.1. XRD analysis of carriers and catalysts

Evidence for the formation of ordered mesostructure is provided by small-angle XRD patterns shown in Figure 1 (1). As shown in the figure, both OMA and OMA-3Ca showed a group of extremely strong diffraction peaks in the range of 0.7^{o}-0.9^{o} and another group of poorly resolved diffraction peaks around 1.5^{o}, respectively, which according to the TEM observation (refer to Figure 3), could be attributed to *p6mm* symmetry. NPA-3Ca synthesized without P123 template performed no diffraction peak in small-angle range, suggesting the significant role of P123 template in constructing ordered mesopore structure. The wide-angle XRD patterns (Figure 1 (2)) of the OMA, OMA-3Ca, and NPA-3Ca carriers could be indexed to γ-Al_2O_3 (JCPDS Card No. 10–0425). There was no CaO characteristic peak observed for OMA-3Ca and NPA-3Ca, indicating the high dispersion among the alumina matrix due to the favorable feature of one-pot method. Compared with OMA, both OMA-3Ca and NPA-3Ca exhibited relatively weaker γ-Al_2O_3 diffraction intensities. This phenomenon implied that the presence of Ca did not favor the phase transformation from amorphous state towards γ phase alumina.

Figure 1 (3) presented the XRD patterns of supported catalysts. It was of great interest to learn that the characteristic peaks for NiO were absent and only γ-Al_2O_3 diffraction peaks could be observed for 5%Ni/OMA and 5%Ni/OMA-3Ca samples. This indicated that the Ni species were highly dispersed among the mesoporous channels. On the contrary, 5%Ni/NPA-3Ca without ordered mesoporous structure behaved apparent NiO diffraction peaks (JCPDS Card No. 78 – 0429), suggesting the poor dispersion over the surface of NPA-3Ca. Therefore, the presence of mesoporous structure played an important role in promoting the dispersion of Ni species for supported catalysts.

Besides, the XRD patterns of the as-reduced catalysts were also shown in Figure 1 (4). As shown in the figure, the diffraction peaks of γ-Al_2O_3 and metallic Ni (JCPDS Card No. 87-0712) were obviously observed. Compared with their corresponding as-synthesized catalysts, all the as-reduced samples behaved much stronger γ-Al_2O_3 diffraction peaks. This phenomenon suggested that the process of phase transformation from amorphous to γ phase alumina took place when the catalysts were reduced at 800 ^{o}C high temperature. Furthermore, it was noticeable that the 5%Ni/NPA-3Ca sample performed much greater metallic Ni diffraction peaks than 5%Ni/OMA and 5%Ni/OMA-3Ca. Therefore, the presence of mesoporous structure was beneficial to the stabilization of the metallic Ni nanoparticles. It might be the confinement effect of the mesoporous channels that contributed to suppressing the thermal growth of the Ni active sites.

3.2. N_2 adsorption-desorption analysis for carriers and catalysts

The porosities of the carriers and catalysts were distinctly confirmed by the analysis of nitrogen adsorption-desorption analyses. Their isotherms (panel A) and BJH pore size distribution curves (panel B) were observed in Figure 2. As shown in Figure 2 (1) panel A, OMA and OMA-3Ca carriers exhibited type IV isotherms with a H1 shaped hysteresis loops, which signified the presence of uniform cylindrical mesoporous channels. However, there was no sign of hysteresis loop for NPA-3Ca, suggesting the absence of evident mesostructure. Further, both OMA and OMA-3Ca possessed greatly narrow pore size distributions around 9.5 nm. On the contrary, the pore size distribution for NPA-3Ca was extremely wide, once again illuminating the absence of uniform mesopores.

Besides, the isotherms and pore size distribution curves for Ni based catalysts were depicted in Figure 2 (2). Dissimilar to OMA and OMA-3Ca with H1 hysteresis loops, 5%Ni/OMA and 5%Ni/OMA-3Ca catalysts performed IV H2 typed hysteresis loops, which were the typical features of mesopores with “ink-bottle” shapes. The reason for this might derive from the deformation of the mesoporous channels from “cylindrical” shape to “ink-bottle” shape during the process of catalyst preparation. Furthermore, these two catalysts also displayed very narrow pore size distributions around 5.5 nm. Compared with their corresponding carriers, their average pore diameter suffered some decline, illustrating the occurrence of the shrinkage of the mesoporous skeleton after the loading of NiO and following calcination process. As for 5%Ni/NPA-3Ca catalyst, it behaved inconspicuous hysteresis loop and wide pore size distribution.

The detailed data related with the structural properties of carriers and catalysts were summarized in Table 1. As shown in the table, OMA-3Ca and OMA carriers with mesostructure were provided with large specific surface areas up to 225.0 m^2/g, large volumes up to 0.538 cm^3/g, and pore diameters around 9.5 nm. However, the NPA-3Ca carrier without obvious mesostructure behaved much smaller surface area and pore volume than those of mesoporous carriers, further confirming the important role of P123 template in improving textural properties. As for the mesoporous catalysts, in comparison with their corresponding carriers, their pore volumes and pore diameters suffered some decline after loading Ni species and subsequent calcination. The reason for this might be that the loaded Ni species took up some space of the mesoporous channels and the mesoporous channels suffered some shrinkage during the process of preparing catalysts. It was also surprising to find that 5%Ni/NPA-3Ca exhibited much bigger surface area and pore volume than NPA-3Ca's, which might be attributed to the appearance of γ phase alumina in the catalyst. But its specific reason was remain unclear.

3.3. TEM analysis of carriers and catalysts

In order to further confirm the presence of ordered mesoporous structure in OMA and OMA-3Ca carriers, their TEM images had been taken. As shown in Figure 3, the highly ordered cylindrical pores viewed along [1 1 0] orientation were observed over different parts of OMA and OMA-3Ca, revealing a high degree of periodicity in large domains. The results of TEM observation were in good agreement with those of small-angle XRD and N_2 adsorption-desorption measurements. Besides, EDX measurements of the ordered mesostructure domains for these two samples were carried out and their profiles were shown in the insets of Figure 3 (a) and (c). The characteristic peaks for C, O, Cu, Al elements were clearly observed over OMA sample. The signal peaks for C, Cu elements came from the holder and copper mesh of the sample. The intense peaks for O, Al elements once again illustrated the main composition of mesoporous wall was constituted by Al_2O_3, which had been proved by XRD. As for the EDX profile of OMA-3Ca, apart from the peaks for C, O, Cu, Al, the characteristic peaks for Ca element were also noticeable, implying Ca element was successfully introduced into ordered mesoporous framework by the present one-pot EISA strategy. The SAED patterns of the ordered domains were also provided in the inlets of Figure 3 (b) and (d). But their diffraction rings were very blurry, indicating that the crystallinity of the mesoporous frameworks was not very good. Generally, the results of the SAED were well consistent with the peak broadening of the XRD patterns (refer to Figure 1 (2)).

The morphology analysis of the 5%Ni/OMA and 5%Ni/OMA-3Ca catalysts was also performed and their TEM images were displayed in Figure 4. Compared with their corresponding carriers, the orderliness of the mesopores for catalysts suffered from some damages during the process of catalyst preparation, which had been reflected in the shapes of their isotherms (see Figure 2 (2) panel A). However, the ordered mesopores along [1 1 0] direction for different parts of the catalysts were still visible, demonstrating excellent thermal stability of OMA and OMA-3Ca carriers. Besides, it was worth noting that no evident NiO clusters were observed in the images, illustrating the high dispersion of NiO species among the mesoporous channels. This phenomenon further explained the absence of NiO diffraction peaks in the XRD patterns of mesoporous catalysts (refer to Figure 1 (3)). However, their EDX profiles (inlets of Figure 4 (a) and (d)) confirmed that Ni species had been successfully loaded on the carriers due to the presence of Ni characteristic peak. These phenomena indicated the high dispersion of Ni species over mesoporous supports. In ordered to study the crystalline properties of the catalysts, SAED (inlets of Figure 4 (b) and (e)) and high resolution TEM measurements (Figure 4 (c) and (f)) were also carried out, in which no diffraction rings as well as crystal lattices were clearly observed, respectively. This indicated that the crystallinity of these two mesoporous catalysts was not very good, which was well consistent with the results of above XRD analysis (Figure 1 (3))

3.4. CO_2-TPD analysis of carriers

CO_2-TPD analysis was carried out to determine the surface basicity of the catalyst carriers. The CO_2-TPD profiles of the OMA, OMA-3Ca, and NPA-3Ca were detailedly compared in Figure 5. As shown in the figure, the OMA-3Ca performed the strongest CO_2 desorption peak, while the NPA-3Ca displayed the weakest CO_2 desorption peak. Compared with OMA, it was the modification of Ca that greatly intensified the basicity of OMA-3Ca's framework. The incorporation of Ca significantly increased the number of Lewis basic sites. As regards the NPA-3Ca, it was the absence of mesostructure that dramatically weakened the basicity of NPA-3Ca. As a result, the CO_2 molecules were not able to get access to the inner Ca basic sites of the NPA-3Ca bulk, finally leading to the decrease in basicity. Further, all the samples performed CO_2 desorption peaks in different temperature ranges. Generally, it was believed that CO_2 adsorbed on weaker basic sites would be desorbed at lower temperatures and that adsorbed on stronger basic sites would be desorbed at higher temperatures. It was noticeable that there were the strong and broad peaks around 170-200 ^{o}C for all the samples. They might be attributed to weakly chemisorbed CO_2 as well as physically adsorbed CO_2 based on pioneer literatures [35, 36]. It was also of great interest to find that, with the addition of the Ca, the positions of these peaks suffered some migration towards higher temperatures from 174 ^{o}C to 192 ^{o}C or 195 ^{o}C. This indicated that the incorporation of Ca modifier contributed to intensifying the chemisorption of CO_2. As for the peaks in 405-795 ^{o}C and 795-1120 ^{o}C regions, they ought to be attributed to basic sites with moderate and strong intensities, respectively. As mentioned above, these carriers were provided with abundant Lewis basic sites with different intensities.

3.5. H_2-TPR and XPS analyses of catalysts

H_2-TPR was utilized to determine the interactions between Ni species and catalyst supports. Their results were shown in Figure 6 (1). As displayed in the figure, all the samples except for 5%Ni/OMA performed two apparent reduction peaks around 900 and 1000 ^{o}C, respectively. As a comparison, 5%Ni/OMA only presented one reduction peak at 924 ^{o}C. However, no reduction peaks appeared in the range of 300-400 ^{o}C, suggesting the absence of NiO species in free or dissociated state [37, 38]. These evidences proved that the strong interactions between Ni species and the supports had been established. The reduction peaks around 900 ^{o}C and 1000 ^{o}C, they could be attributable to the reduction of surface and bulk nickel species, respectively. It was speculated that $NiAl_2O_4$ spinel-like species might be formed on the surface of the catalysts because of the high reduction temperature. It was also of great interest to notice that the reduction temperature of the first reduction peaks for 5%Ni/OMA-3Ca (897 ^{o}C) and 5%Ni/NPA-3Ca (868 ^{o}C) were a little lower than that for 5%Ni/OMA (924 ^{o}C). In other words, the presence of CaO and mesoporous structure might make the reduction of Ni^{2+} become a little easier. As for the 5%Ni/OMA-3Ca, the reason for this might originate from that the incorporation of CaO would compete with the process of forming $NiAl_2O_4$ spinel-like species ($NiO + Al_2O_3 \rightarrow NiAl_2O_4$) by participating in the following reaction: $CaO + Al_2O_3 \rightarrow CaAl_2O_4$. Besides, as for the 5%Ni/NPA-3Ca, the absence of mesoporous structure might be the main reason that caused the weak interaction between the Ni species and the support. Specifically, there might not be sufficient surface Al_2O_3 sites to participate in the process related with the formation of $NiAl_2O_4$ spinel-like species ($NiO + Al_2O_3 \rightarrow NiAl_2O_4$) due to low surface area and small pore volume [39]. Besides, it was easy to find in the figure that 5%Ni/NPA-3Ca could be initially reduced at 535 ^{o}C, which was much lower than 5%Ni/OMA and 5%Ni/OMA-3Ca (around 624 ^{o}C). This implied that the interaction between Ni and NPA-3Ca was relatively weaker than those between Ni and mesoporous carriers. The real state of the Ni species over the carriers would be specifically studied by the following XPS analysis.

The XPS profiles of Ni2p element for above-mentioned catalysts were displayed in Figure 6 (2). As shown in the figure, these XPS curves were different with each other for $Ni2p_{3/2}$ binding energy. But their $Ni2p_{3/2}$ peaks were all located in the range of 855.50-856.50 eV. Commonly, the $Ni2p_{3/2}$ binding energy of NiO in free or dissociated state was about 853.30 eV, which was much less than those of the present catalysts [40, 41]. Therefore, the oxidation state of the surface Ni element was performed in the form of Ni^{2+}. As for 5%Ni/OMA, its $Ni2p_{3/2}$ peak was centered on 856.23 eV and accompanied by a satellite peak, which was the typical feature of $NiAl_2O_4$ spinel species [42, 43]. This phenomenon implied that $NiAl_2O_4$ spinel-like species had been form over the surface of the 5%Ni/OMA catalyst. Compared with 5%Ni/OMA, 5%Ni/OMA-3Ca behaved similar profile in the shape. But the $Ni2p_{3/2}$ peak as well as its satellite peak migrated towards lower binding energies with the modification of Ca. As discussed in H_2-TPR analysis, the addition of Ca modifier might influence the formation of $NiAl_2O_4$ spinel-like species. Therefore, the present $Ni2p_{3/2}$ peak and its satellite peak might derive from the overlapping of typical peaks for NiO and $NiAl_2O_4$. However, dissimilar to 5%Ni/OMA and 5%Ni/OMA-3Ca, 5%Ni/NPA-3Ca performed greatly different Ni2p spectrum in the shape, specifically a $Ni2p_{3/2}$ peak centered on 856.08 eV and a satellite peak around 859.78 eV. This phenomenon suggested that the absence of mesoporous alumina matrix might block the formation of $NiAl_2O_4$ on surface. Therefore, these peaks might be attributed to the overlapping of NiO and Ni_2O_3 species. Besides, it was worth noting that 5%Ni/NPA-3Ca exhibited the strongest peak intensity, implying the highest concentration of surface NiO species among these three catalysts. This phenomenon also demonstrated the poor dispersion of NiO species, which had been testified by XRD analysis. In summary, the XPS analysis was in good agreement with the results of the H_2-TPR as well as XRD characterization.

3.6. Catalytic performances of the CRM reaction over the catalysts

The long-term stability tests of over these catalysts were examined under given reaction conditions: CH_4/CO_2 = 1, 700 ^oC, GHSV = 15000 mL/(g·h), 1 atm and their experimental results were shown in Figure 7. As displayed in the Figure 7 (1) and (2), both 5%Ni/OMA and 5%Ni/OMA-3Ca catalysts with ordered mesoporous structures performed both high catalytic activities and greatly stable catalytic stabilities during 100 h time on stream; in contrast, 5%/NPA-3Ca catalyst without evident mesoporous framework suffered severe decline in CH_4, CO_2 conversions during 100 h long-term stability test. The higher catalytic activities of the mesoporous catalysts than 5%Ni/NPA-3Ca ought to be owing to advantages of their structural properties, such as large surface areas, big pore volumes, uniform pore channels, etc, which would provide the gaseous reactants with more "accessible" Ni active sites.

However, the most significant problem met with CRM reaction was the rapid deactivation of catalyst derived from carbon deposition and thermal sintering of the Ni active centers. It was widely considered that Ni particle with smaller size possessed better ability to suppress carbon deposition [4, 21]. But controlling Ni particles within nano-size was not an easy thing. Because the thermal sintering of Ni particles easily took place under the conditions of CRM reaction. As for 5%Ni/OMA and 5%Ni/OMA-3Ca mesoporous catalysts, the "confinement effect" of the mesoporous channels would effectively inhibit the growth of Ni nanoparticles and confine them within nanometer size during the processed of reduction and reaction. As a result, their catalytic stabilities were greatly improved due to the "size effect" of Ni nanoparticles.

Besides, it was noticeable in Figure 7 (1) and (2) that CO_2, CH_4 conversions of 5%Ni/OMA-3Ca were higher than those of 5%Ni/OMA. It was the introduction of Ca basic modifier that contributed to this. Typically, incorporating Ca atoms into mesoporous alumina framework would intensify the chemisorption of CO_2. One the one hand, the chemisorption of the CO_2 would activate CO_2 molecule and increase the concentration of CO_2 on the surface of the catalyst, which was finally beneficial to improve the conversions of CO_2 and CH_4. On the other hand, the presence of basic modifier would promote the process of eliminating carbon deposition by accelerating the reaction: $CO_2 + C \rightarrow 2CO$. As a result, it would enhance the catalytic stability of the catalyst.

The H_2/CO ratios for these three catalysts during 100 h long-term stability test were shown in Figure 7 (3). It was of great interest to find that all the H_2/CO ratios were lower than stoichiometric ratio (1.0) of CRM reaction. The reason for this might derive from the concomitance of the reverse water-gas shift (RWGS), which consumed H_2 and generated CO. As for 5%Ni/OMA and 5%Ni/OMA-3Ca mesoporous catalysts, their H_2/CO ratios were generally steady and regularly verified in an oscillating way around 0.80, illuminating the periodic cycle of carbon deposition reaction and elimination reaction [9]. However, the H_2/CO ratio over 5%Ni/NPA-3Ca catalyst without evident mesostructure initially suffered rapid decline from 0.87 to 0.75 in the first 10 h, implying that the balance between carbon deposition and coke elimination could not be achieved. Therefore, the coke deposition over 5%Ni/NPA-3Ca would be very serious and suffer quick deactivation, which had been confirmed in Figure 7 (1) and (2).

In summary, both mesopore structure and Ca basic modifier played significant roles in improving the catalytic activity and stability of Ni based catalyst for CRM reaction.

3.7. XRD analysis of 100 h endurance-tested catalysts

Figure 8 gave the XRD patterns of 100 h endurance-tested catalysts. As shown in the figure, the 5%Ni/NPA-3Ca without ordered mesoporous structure performed much stronger metallic Ni and graphite carbon diffraction peaks than 5%Ni/OMA and 5%Ni/OMA-3Ca mesoporous catalysts. This phenomenon implied that the mesoporous structure played important roles in inhibiting the thermal agglomeration of the metallic active centers and coke deposition. Specifically, the “confinement effect” of the mesoporous channels could contribute to the stabilization of the Ni nanoparticles. As a result, the Ni active center in nano-size was provided with reinforced ability of coke suppression according to previous literatures [4, 21]. Besides, as for the mesoporous catalysts, the 5%Ni/OMA catalyst without basic modifier behaved relatively stronger graphite carbon peak than 5%Ni/OMA-3Ca catalyst. Its reason might be derived from the presence of CaO basic modifier, which would strengthen the processes of CO_2 chemisorption and activation. As a result, the process of coke elimination ($C + CO_2 \rightarrow 2CO$) was accelerated, which would be further proved by the following TG analysis.

3.8. N_2 adsorption-desorption analysis of 100 h endurance-tested catalysts

In order to study the thermal stability of mesostructure for the mesoporous catalysts, N_2 adsorption-desorption analysis of 100 h endurance-tested catalysts was carried out. Their isotherms and pore size distribution curves were shown in Figure 9. As shown in the figure, it could be observed that the 100 h endurance-tested 5%Ni/OMA and 5%Ni/OMA-3Ca exhibited IV type with H2 shaped hysteresis loops and very narrow pore size distribution around 6.5 nm, which were closely similar with their corresponding as-prepared catalysts (refer to Figure 2 (1)). These phenomena suggested that the mesoporous structure of the catalysts were not seriously destroyed under the severe conditions during the processes of catalyst reduction and CRM reaction, illustrating the good thermal stability of the mesostructure. Besides, the structural properties of the catalysts were also summarized in Table 1. Compared with the as prepared catalysts, the specific surface areas and pore volumes of 100 h spent samples suffered some decrease. The reason for this might be that the coke deposition over the catalyst surface blocked the mesopore channels during the process of CRM reaction. Generally, these mesoporous catalysts were provided with enough thermal stability to endure the severe condition of CRM reaction.

3.9. TG analysis of 100 h endurance-tested catalysts

The amounts of the coke of the 100 h endurance-tested catalysts were determined by TG analysis. The TG curves were depicted in Figure 10 and their general trends were all downwards with the increase of the temperature, which was caused by the gradual combustion of coke. As displayed in the figure, the weight losses over 5%Ni/OMA, 5%Ni/OMA-3Ca, and 5%Ni/NPA-3Ca samples were 8.2%, 9.6%, and 24.2%, respectively. Therefore, it was noticeable to learn that the mesoporous catalysts behaved much better abilities of coke resistance than 5%Ni/NPA-3Ca. The reason for this ought to be attributed to the effect of the mesoporous channels on inhibiting the growth of Ni particles via its “confinement effect” [33]. The Ni particles in nano size would have enhanced ability of suppressing the coke formation.

As for the spent mesoporous catalysts, the coke over 5%Ni/OMA-3Ca (8.2%) was less than that over 5%Ni/OMA (9.6%), which should be owing to the addition of Ca basic modifier. Introducing Ca into the mesoporous framework would greatly increase the number of the surface basic sites, which had been proved by above CO_2-TPD analysis. Therefore, the chemisorption and activation of CO_2 could be obviously strengthened, which finally accelerated the coke elimination ($C + CO_2 \rightarrow 2CO$) [29].

These phenomena suggested that Ca basic modifier seemed to play less important role than mesoporous structure in suppressing the coke formation. But they were all in favor of the coke suppression, which finally contributed to good catalytic stability.

3.10. TEM analysis of 100 h endurance-tested catalysts

In order to investigate the morphology of the coke over 100 h endurance-tested catalysts and the reason for 5%Ni/NPA-3Ca deactivation, TEM analysis of the 100 h endurance-tested 5%Ni/OMA-3Ca and 5%Ni/NPA-3Ca catalysts were performed. The images were displayed in Figure 11. It was noticeable in Figure 11 (a, b) that no obvious coke was found over the spent 5%Ni/OMA-3Ca catalyst. The size of metallic Ni nanoparticle was about 9.5 nm according to high resolution TEM image in Figure 11 (b). This implied that the “confinement effect” of the mesoporous channels effectively suppressed the thermal sintering of Ni particles during the reaction. As a result, the nano-sized Ni particles had enhanced ability of coke resistance. Besides, the cylindrical pore channels of the 5%Ni/OMA-3Ca had been deformed into wormlike pores after 100 h CRM reaction, which had been testified by N_2 adsorption-desorption analysis of the spent catalysts. As for the spent 5%Ni/NPA-3Ca, its surface coke residue was mainly in the form of carbon nanotubes (see Figure 11 (c, d, e, f, and h)). It also could be observed in Figure 11 (d, e, f, and h) that the metallic Ni partic\les were completely enwrapped or partly encapsulated at the tail end by the multi-wall carbon nanotubes. As a result, the gaseous reactant could not access the Ni active centers, which finally caused the rapid deactivation of the present catalyst.

3.11. Comparison between ordered mesoporous Ni/Al_2O_3-CaO supported catalysts and NiO-CaO-Al_2O_3 composite oxides catalysts

In our previous study, we had successfully prepared ordered mesoporous NiO-CaO-Al_2O_3 composite oxides by one-pot EISA strategy and directly utilized them as the catalysts for CRM reaction [32]. In this catalytic system, both Ni active species and CaO basic modifier were embedded in the mesoporous framework of the catalyst due to the unique property of the one-pot synthesis method. The confinement effect of the mesoporous framework played an important role in limiting the thermal sintering of the Ni nanoparticles during the CRM reaction, which accounted for long catalytic stability of the catalyst. Besides, the effects of the CaO modifier and its loading on improving catalytic performance and suppressing the coke had been systematically investigated. It was found that the catalyst with moderate Ca modification (3 mol %) performed highest catalytic activity and excessive basic modifier would suppress the catalytic activity. Compared with the NiO-Al_2O_3 catalyst without CaO basic modifier, these NiO-CaO-Al_2O_3 catalysts with basic modifier performed much lower surface carbon deposition by accelerating the coke elimination process.

As a comparison, the present ordered mesoporous Ni/Al_2O_3-CaO supported catalysts were prepared using ordered mesoporous Al_2O_3-CaO composite oxides as catalytic carrier via incipient impregnation method. In this catalytic system, only CaO basic modifier was embedded in the mesoporous framework. As for the Ni active sites, they were uniformly dispersed among the mesoporous channels. Compared with the catalyst without mesoporous structure, these mesoporous catalysts performed better catalytic stability. It was the confinement effect of the mesoporous channels that effectively suppressed the thermal sintering of the Ni nanoparticles, which would lead to the long catalytic stability. Similar to ordered mesoporous NiO-CaO-Al_2O_3 catalyst, the presence of CaO basic modifier also acted significant roles in promoting the catalytic performance and suppressing the surface coke.

Generally, as for these two ordered mesoporous catalytic systems, it was easy to learn that the confinement effects of both mesoporous framework (NiO-CaO-Al_2O_3) and mesoporous channel (Ni/Al_2O_3-CaO) played positive roles in stabilizing the Ni nanoparticles during the process of CRM reaction based on above discussion. It was also to conclude that CaO basic modifier played critical role in improving catalytic performance and inhibiting the surface coke by enhancing the chemisorption of the CO_2 for both supported and composite oxide (non-supported) catalysts.

4. Conclusion

In summary, ordered mesoporous CaO-Al_2O_3 composite oxide obtained via improved EISA method had been testified as catalytic supporter for Ni based catalyst toward CRM reaction. It was found that 5%Ni/OMA-3Ca catalyst with both ordered mesostructure and basic modifier behaved better catalytic properties than the comparative catalysts without ordered mesoporous framework (5%Ni/NPA-3Ca) or basic additive (5%Ni/OMA). Therefore, both the ordered mesoporous structure and CaO basic modifier played significant roles in promoting catalytic activity and stability. Specifically, the ordered mesostructure could accommodate the gaseous reactants with more “accessible” active centers, resulting in higher catalytic activity; the confinement effect of the mesopore could effectively suppress the thermal sintering of the Ni nanoparticles, accounting for better catalytic stability. As for the CaO basic modifier, its presence remarkably strengthened the chemisorption of CO_2, which would be beneficial to the processes of CO_2 activation and coke elimination. Besides, it was found that the deactivation of the Ni based catalyst was caused by the coverage of the Ni active centers.

Acknowledgements

The authors sincerely acknowledge the financial support from the National Basic Research Program of PR China (No. 2011CB201404) and the National Natural Science Foundation of China (No. 21133011 and 21373244).

References

1. Z. Hou, J. Gao, J. Guo, D. Liang, H. Lou and X. Zheng, *J. Catal.*, 2007, 250, 331-341.

2. J. T. Richardson and S. A. Paripatyadar, *Appl. Catal.*, 1990, 61, 293-309.

3. J. H. Edwards, *Catal. Today*, 1995, 23, 59-66.

4. M. C. J. Bradford and M. A. Vannice, *Cat. Rev.-Sci. Eng.*, 1999, 41, 1-42.

5. A. T. Ashcroft, A. K. Cheetham, M. L. H. Green and P. D. F. Vernon, *Nature*, 1991, 352, 225-226.

6. M.S. Fan, A. Z. Abdullah and S. Bhatia, *Chemcatchem*, 2009, 1, 192-208.

7. I. Wender, *Fuel Process. Technol.*, 1996, 48, 189-297.

8. P. Eilbracht, L. Barfacker, C. Buss, C. Hollmann, B. E. Kitsos-Rzychon, C. L. Kranemann, T. Rische, R. Roggenbuck and A. Schmidt, *Chem. Rev.*, 1999, 99, 3329-3365.

9. J. M. Wei, B. Q. Xu, J. L. Li, Z. X. Cheng and Q. M. Zhu, *Appl. Catal. A: Gen.*, 2000, 196, L167-L172.

10. M. Levy, R. Levitan, H. Rosin and R. Rubin, *Sol. Energy*, 1993, 50, 179-189.

11. C.J. Liu, J. Ye, J. Jiang and Y. Pan, *Chemcatchem*, 2011, 3, 529-541.

12. M. Garcia-Dieguez, I. S. Pieta, M. C. Herrera, M. A. Larrubia and L. J. Alemany, *Appl. Catal. A: Gen.*, 2010, 377, 191-199.

13. M. M. Yung and J. N. Kuhn, *Langmuir*, 2010, 26, 16589-16594.

14. A. Alubaid and E. E. Wolf, *Appl. Catal.*, 1988, 40, 73-85.

15. C. Batiot-Dupeyrat, G. Valderrama, A. Meneses, F. Martinez, J. Barrault and J. M. Tatibouet, *Appl. Catal. A: Gen.*, 2003, 248, 143-151.

16. V. R. Choudhary, B. S. Uphade and A. A. Belhekar, *J. Catal.*, 1996, 163, 312-318.

17. J. Gallego, C. Batiot-Dupeyrat, J. Barrault and F. Mondragon, *Energy Fuels*, 2009, 23, 4883-4886.

18. G. Sierra Gallego, J. Gallego Marin, C. Batiot-Dupeyrat, J. Barrault and F. Mondragon, *Appl. Catal. A: Gen.*, 2009, 369, 97-103.

19. G. Sierra Gallego, F. Mondragon, J. Barrault, J.M. Tatibouet and C. Batiot-Dupeyrat, *Appl. Catal. A: Gen.*, 2006, 311, 164-171.

20. K. Tomishige, Y. G. Chen and K. Fujimoto, *J. Catal.*, 1999, 181, 91-103.

21. Y. H. Hu, *Catal. Today*, 2009, 148, 206-211.

22. Y. H. Hu and E. Ruckenstein, *Cat. Rev.-Sci. Eng.*, 2002, 44, 423-453.

23. Z. L. Xu, M. Zhen, Y. L. Bi and K. J. Zhen, *Appl. Catal. A: Gen.*, 2000, 198, 267-273.

24. T. H. Gardner, D. Shekhawat, D. A. Berry, M. W. Smith, M. Salazar and E. L. Kugler, *Appl. Catal. A: Gen.*, 2007, 323, 1-8.

25. D. L. Trimm, *Catal. Today*, 1997, 37, 233-238.

26. J. R. Nielsen and D. L. Trimm, *J. Catal.*, 1977, 48, 155-165.

27. R. Yang, C. Xing, C. Lv, L. Shi and N. Tsubaki, *Appl. Catal. A: Gen.*, 2010, 385, 92-100.

28. T. Horiuchi, K. Sakuma, T. Fukui, Y. Kubo, T. Osaki and T. Mori, *Appl. Catal. A: Gen.*, 1996, 144, 111-120.

29. S. Liu, L. Guan, J. Li, N. Zhao, W. Wei and Y. Sun, *Fuel*, 2008, 87, 2477-2481.

30. L. Xu, H. Song and L. Chou, *Appl. Catal. B: Environ.*, 2011, 108, 177-190.

31. L. Xu, H. Song and L. Chou, *Catal. Sci. Technol.*, 2011, 1, 1032-1042.

32. L. Xu, H. Song and L. Chou, *Acs Catal.*, 2012, 2, 1331-1342.

33. N. Sun, X. Wen, F. Wang, W. Wei and Y. Sun, *Energy Environ. Sci.*, 2010, 3, 366-369.

34. Q. Yuan, A.X. Yin, C. Luo, L.D. Sun, Y.W. Zhang, W.T. Duan, H.C. Liu and C.H. Yan, *J. Am. Chem. Soc.*, 2008, 130, 3465-3472.

35. M. Rezaei, S. M. Alavi, S. Sahebdelfar, P. Bai, X. Liu and Z.-F. Yan, *Appl. Catal. B: Environ.*, 2008, 77, 346-354.

36. L. Pino, A. Vita, F. Cipiti, M. Lagana and V. Recupero, *Appl. Catal. B: Environ.*, 2011, 104, 64-73.

37. W. S. Dong, H. S. Roh, K. W. Jun, S. E. Park and Y. S. Oh, *Appl. Catal. A: Gen.*, 2002, 226, 63-72.

38. S. Zhang, J. Wang, H. Liu and X. Wang, *Catal. Commun.*, 2008, 9, 995-1000.

39. J. A. C. Dias and J. M. Assaf, *Catal. Today*, 2003, 85, 59-68.

40. Y. S. Oh, H. S. Roh, K. W. Jun and Y. S. Baek, *Int. J. Hydrogen Energy*, 2003, 28, 1387-1392.

41. A. P. Grosvenor, M. C. Biesinger, R. S. Smart and N. S. McIntyre, *Surf. Sci.*, 2006, 600, 1771-1779.

42. K. T. Ng and D. M. Hercules, *J. Phys. Chem.*, 1976, 80, 2094-2102.

43. Y. L. Chu, S. B. Li, J. Z. Lin, J. F. Gu and Y. L. Yang, *Appl. Catal. A: Gen.*, 1996, 134, 67-80.

Table caption:

Table 1. Textural properties of the catalytic carriers, Ni based catalysts, and 100 h endurance-tested catalysts.

Figure captions:

Figure 1. (1) Small-angle X-ray diffraction and **(2)** Wide-angle X-ray diffraction patterns of the catalytic carriers: **(a)** OMA, **(b)** OMA-3Ca, **(c)** NPA-3Ca;

(3) X-ray diffraction patterns of Ni based catalysts: **(a)** 5%Ni/OMA, **(c)** 5%Ni/OMA-3Ca, **(c)** 5%Ni/NPA-3Ca;

(4) X-ray diffraction patterns of as-reduced Ni based catalysts: **(a)** 5%Ni/OMA, **(c)** 5%Ni/OMA-3Ca, **(c)** 5%Ni/NPA-3Ca.

Figure 2. Isotherms **(panel A)** and pore size distributions **(panel B)** of **(1)** catalytic carriers and **(2)** corresponding Ni based catalysts.

Figure 3. TEM images and EDX measurements of the catalytic carriers: **(a)** and **(b)** OMA, **(c)** and **(d)** OMA-3Ca.

Figure 4. TEM images and EDX measurements of the Ni based catalysts: **(a)**, **(b)**, and **(c)** 5%Ni/OMA, **(d), (e)** and **(f)** 5%Ni/OMA-3Ca.

Figure 5. CO_2-TPD profiles of the catalytic carriers: **(a)** OMA, **(b)** OMA-3Ca, **(c)** NPA-3Ca.

Figure 6. (1) H_2-TPR profiles and **(2)** XPS spectra of Ni2p for Ni based catalysts: **(a)** 5%Ni/OMA, **(b)** 5%Ni/OMA-3Ca, **(c)** 5%Ni/NPA-3Ca.

Figure 7. 100 h long-term stability tests over the Ni based catalysts: **(1)** CH_4 conversion, **(2)** CO_2 conversion, and **(3)** H_2/CO ratio; reaction conditions: $CH_4/CO_2 = 1$, GHSV = 15000 mL/(g·h), 700 ^{o}C, 1 atm.

Figure 8. XRD patterns of the 100 h endurance-tested catalysts: **(a)** 5%Ni/OMA, **(b)** 5%Ni/OMA-3Ca, and **(c)** 5%Ni/NPA-3Ca catalysts.

Figure 9. Isotherms **(1)** and pore size distributions **(2)** of the 100 h endurance-tested catalysts.

Figure 10. TG curves of the 100 h endurance-tested catalysts: **(a)** 5%Ni/OMA, **(b)** 5%Ni/OMA-3Ca, and **(c)** 5%Ni/NPA-3Ca catalysts.

Figure 11. TEM pictures and EDX measurements of the 100 h endurance-tested catalysts: **(a), (b)** 5%Ni/OMA-3Ca; **(c)**, **(d)**, **(e)**, **(f)**, **(g)**, **(h)**, and **(i)** 5%Ni/NPA-3Ca.

Table 1

Samples	**Specific Surface Area (m^2/g)**	**Pore Volume (cm^3/g)**	**Average Pore Diameter (nm)**	**Isotherm Type**
OMA	224.957	0.538	9.457	IV H1
OMA-3Ca	169.864	0.480	9.543	IV H1
NPA-3Ca	17.150	0.018	—	—
5%Ni/OMA	213.268	0.293	5.597	IV H2
5%Ni/OMA-3Ca	178.048	0.249	5.607	IV H2
5%Ni/NPA-3Ca	43.897	0.072	—	IV H3
100 h endurance-tested 5%Ni/OMA	156.837	0.267	6.573	IV H2
100 h endurance-tested 5%Ni/OMA-3Ca	124.522	0.221	6.557	IV H2
100 h endurance-tested 5%Ni/NPA-3Ca	40.46	0.252	—	IV H3

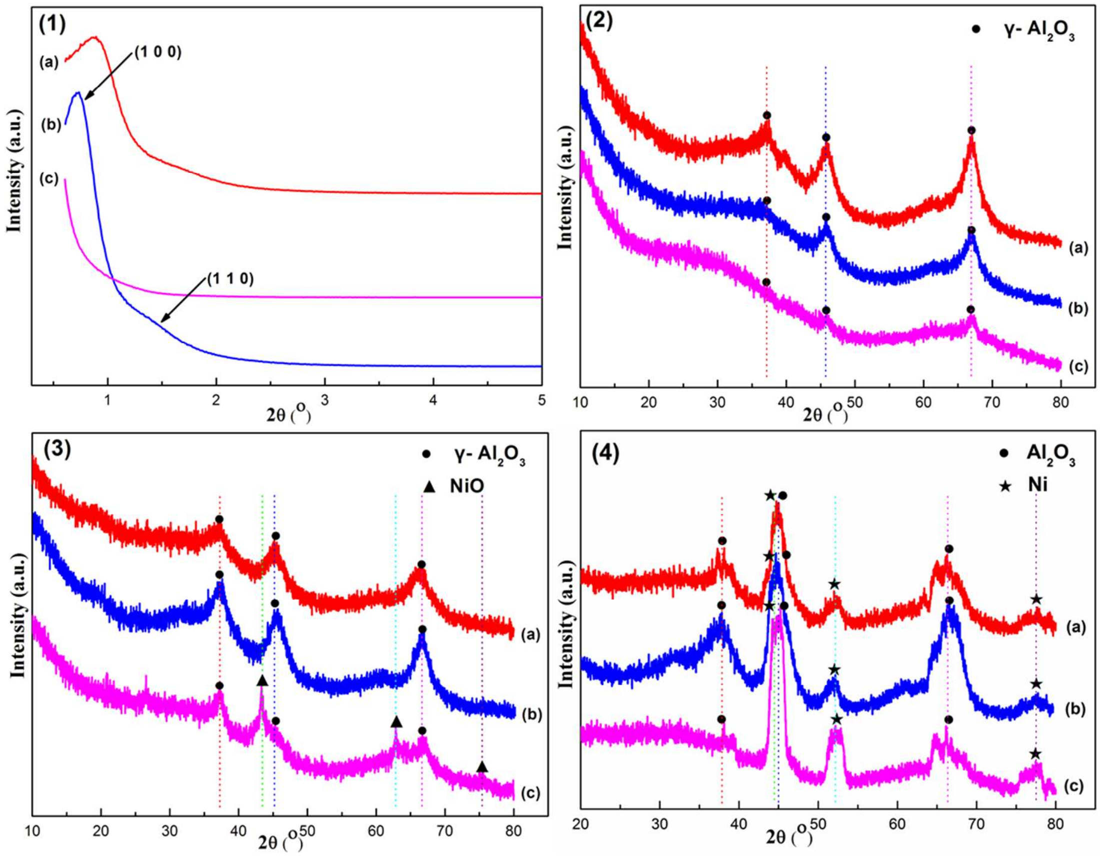
(1)
(a)
(b)
(c)
(1 0 0)
(1 1 0)
Intensity (a.u.)
2θ (°)
1
2
3
4
5
(2)
● γ- Al2O3
(a)
(b)
(c)
Intensity (a.u.)
2θ (°)
10
20
30
40
50
60
70
80
(3)
● γ- Al2O3
▲ NiO
(a)
(b)
(c)
Intensity (a.u.)
2θ (°)
(4)
● Al2O3
★ Ni
(a)
(b)
(c)
Intensity (a.u.)
2θ (°)

Figure 1

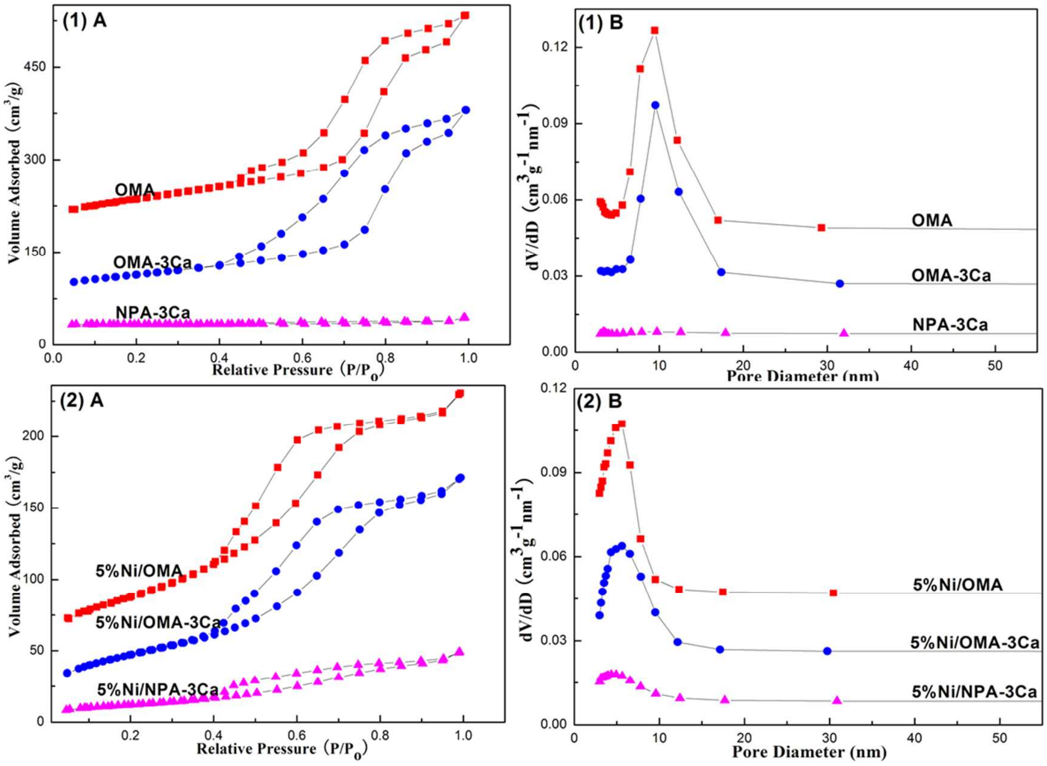
(1) A
Volume Adsorbed (cm^3/g)
Relative Pressure (P/P$_0$)
OMA
OMA-3Ca
NPA-3Ca
(1) B
dV/dD (cm^{3}g^{-1}nm^{-1})
Pore Diameter (nm)
OMA
OMA-3Ca
NPA-3Ca
(2) A
Volume Adsorbed (cm^3/g)
Relative Pressure (P/P$_0$)
5%Ni/OMA
5%Ni/OMA-3Ca
5%Ni/NPA-3Ca
(2) B
dV/dD (cm^{3}g^{-1}nm^{-1})
Pore Diameter (nm)
5%Ni/OMA
5%Ni/OMA-3Ca
5%Ni/NPA-3Ca

Figure 2

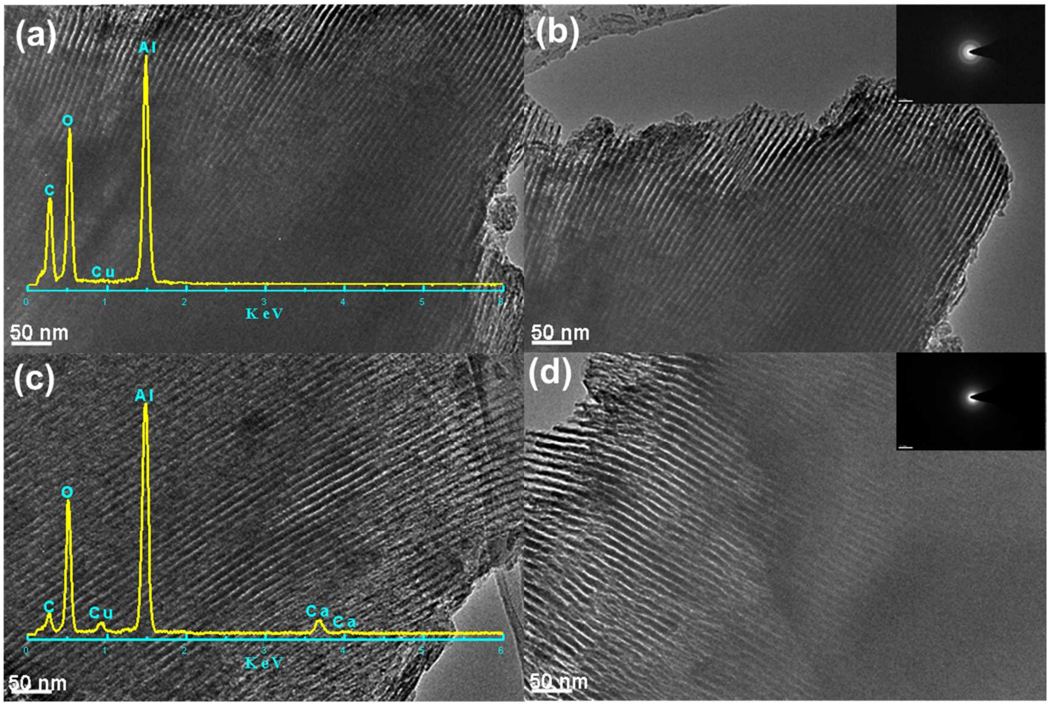

Figure 3

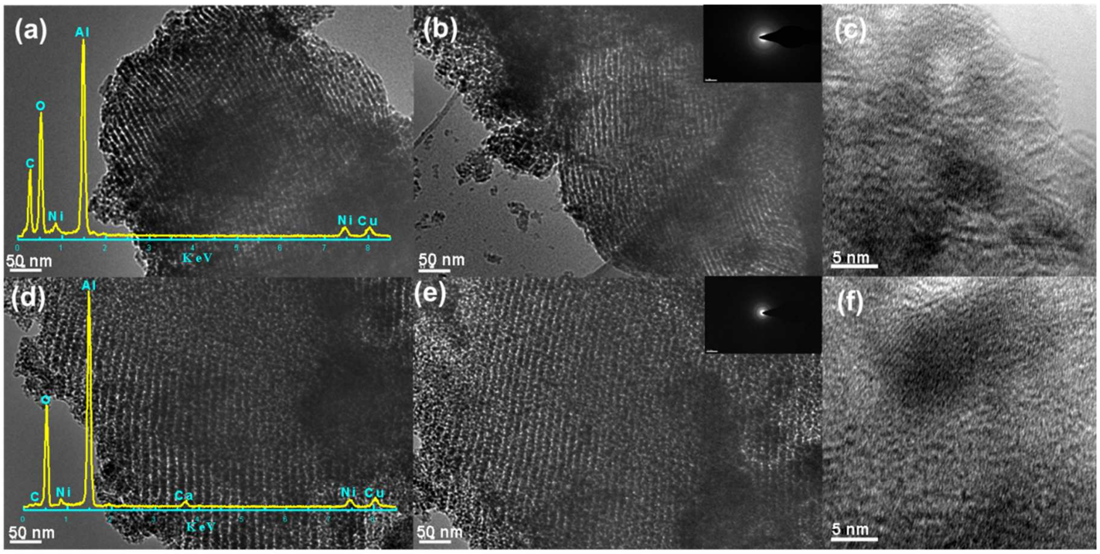
(a)
Al
O
C
Ni
Ni Cu
KeV
50 nm
(b)
50 nm
(c)
5 nm
(d)
Al
O
C
Ni
Ca
Ni Cu
KeV
50 nm
(e)
50 nm
(f)
5 nm

Figure 4

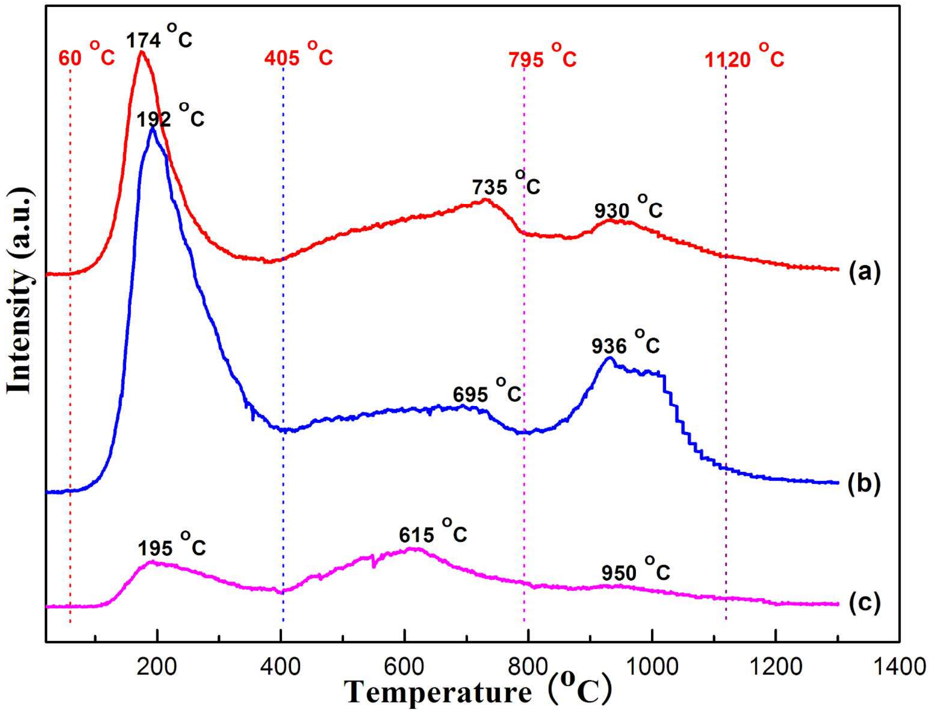
60 °C
174 °C
405 °C
795 °C
1120 °C
192 °C
735 °C
930 °C
936 °C
695 °C
195 °C
615 °C
950 °C
(a)
(b)
(c)
Intensity (a.u.)
Temperature (°C)
200
400
600
800
1000
1200
1400

Figure 5

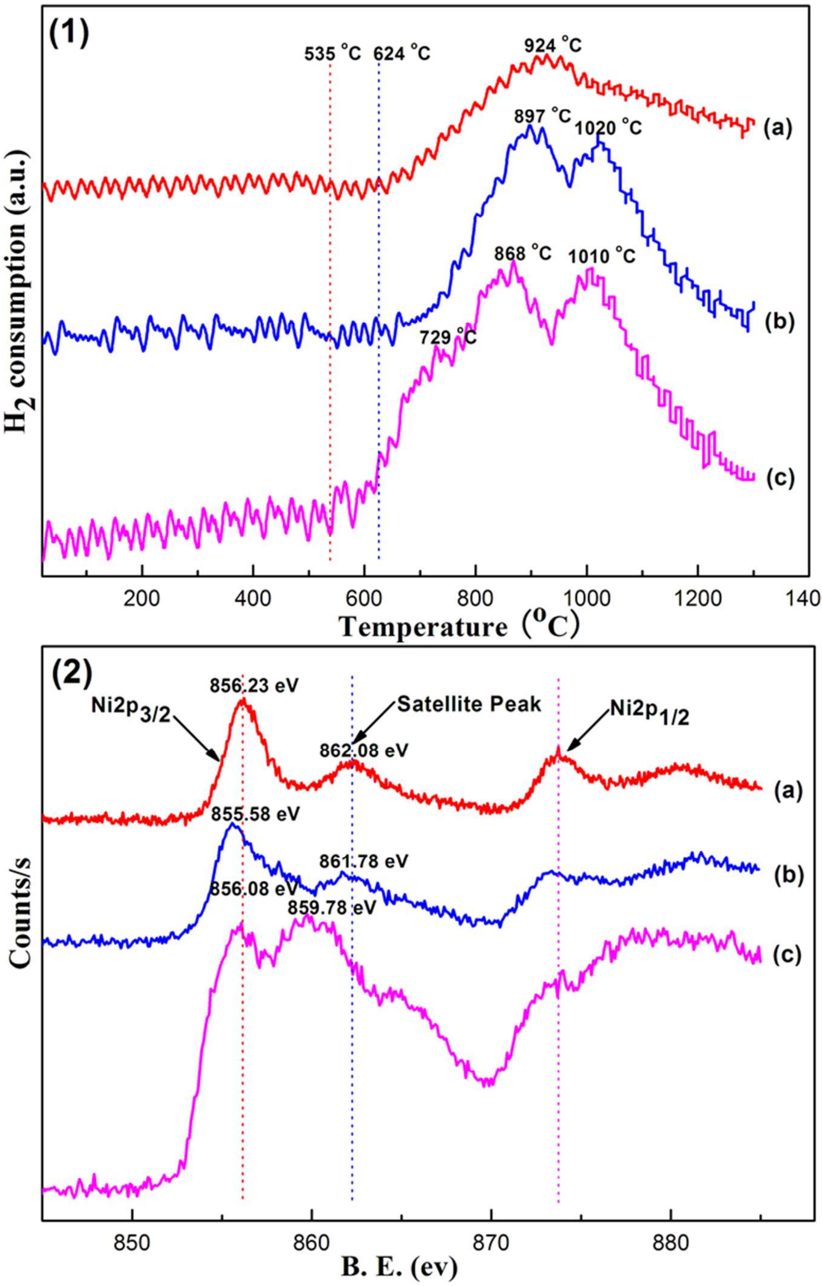
(1)
535 °C
624 °C
924 °C
897 °C
1020 °C
868 °C
1010 °C
729 °C
(a)
(b)
(c)
H$_2$ consumption (a.u.)
200
400
600
800
1000
1200
1400
Temperature (°C)
(2)
Ni2p$_{3/2}$
856.23 eV
Satellite Peak
Ni2p$_{1/2}$
862.08 eV
855.58 eV
861.78 eV
856.08 eV
859.78 eV
(a)
(b)
(c)
Counts/s
850
860
870
880
B. E. (ev)

Figure 6

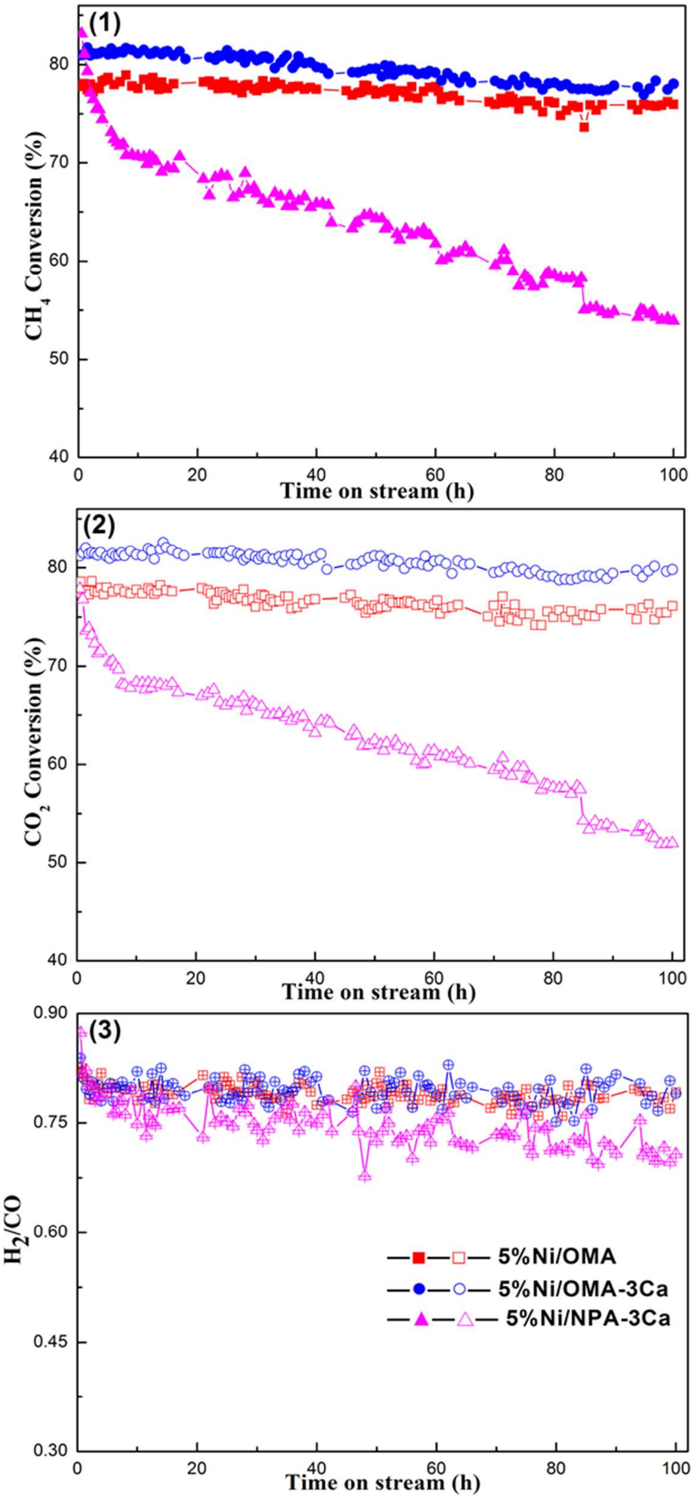
(1)
CH$_4$ Conversion (%)
80
70
60
50
40
0
20
40
60
80
100
Time on stream (h)
(2)
CO$_2$ Conversion (%)
80
70
60
50
40
0
20
40
60
80
100
Time on stream (h)
(3)
H$_2$/CO
0.90
0.75
0.60
0.45
0.30
0
20
40
60
80
100
Time on stream (h)
5%Ni/OMA
5%Ni/OMA-3Ca
5%Ni/NPA-3Ca

Figure 7

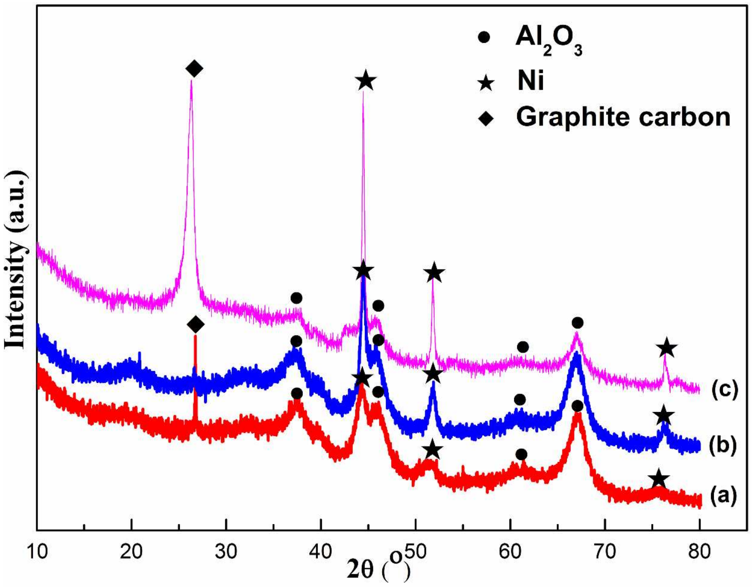
● Al2O3
★ Ni
◆ Graphite carbon
Intensity (a.u.)
2θ (o)
10
20
30
40
50
60
70
80
(a)
(b)
(c)

Figure 8

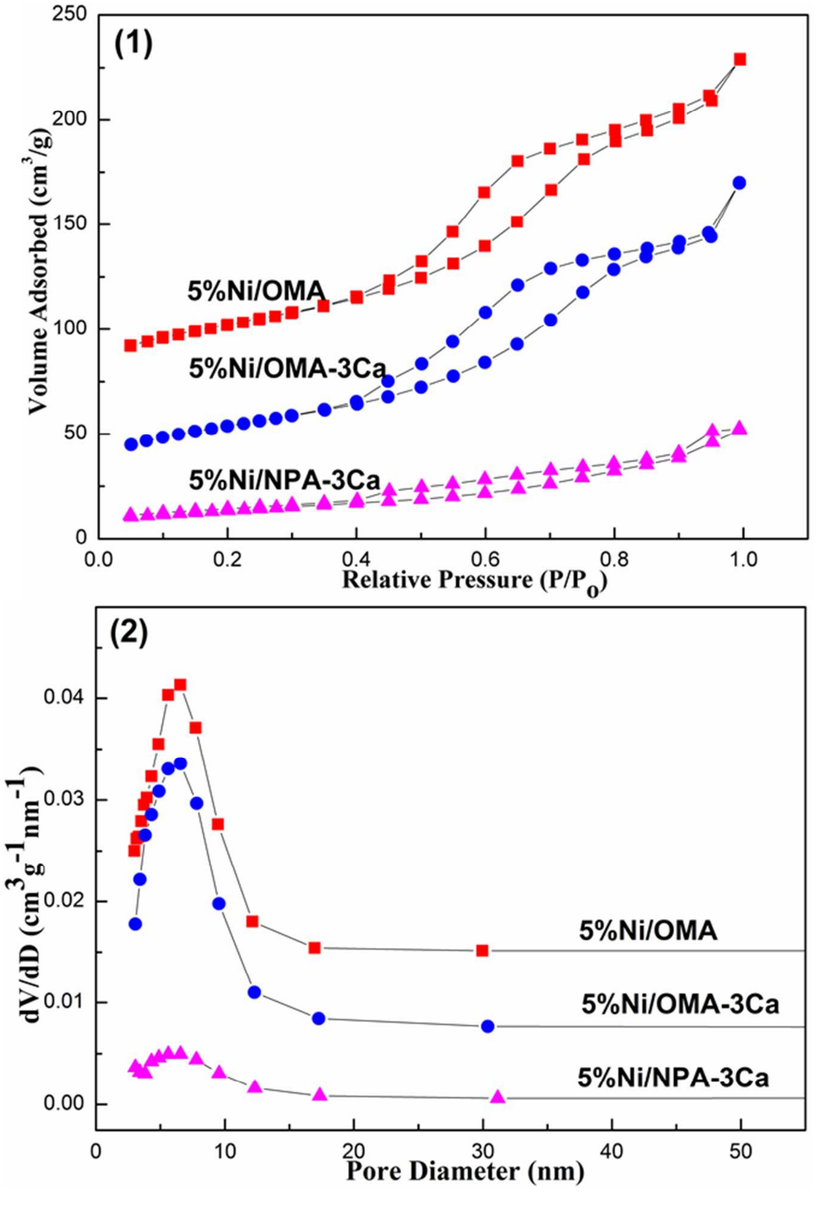
(1)
Volume Adsorbed (cm^3/g)
250
200
150
100
50
0
5%Ni/OMA
5%Ni/OMA-3Ca
5%Ni/NPA-3Ca
0.0
0.2
0.4
0.6
0.8
1.0
Relative Pressure (P/P$_o$)
(2)
dV/dD (cm^{3}g^{-1}nm^{-1})
0.04
0.03
0.02
0.01
0.00
5%Ni/OMA
5%Ni/OMA-3Ca
5%Ni/NPA-3Ca
0
10
20
30
40
50
Pore Diameter (nm)

Figure 9

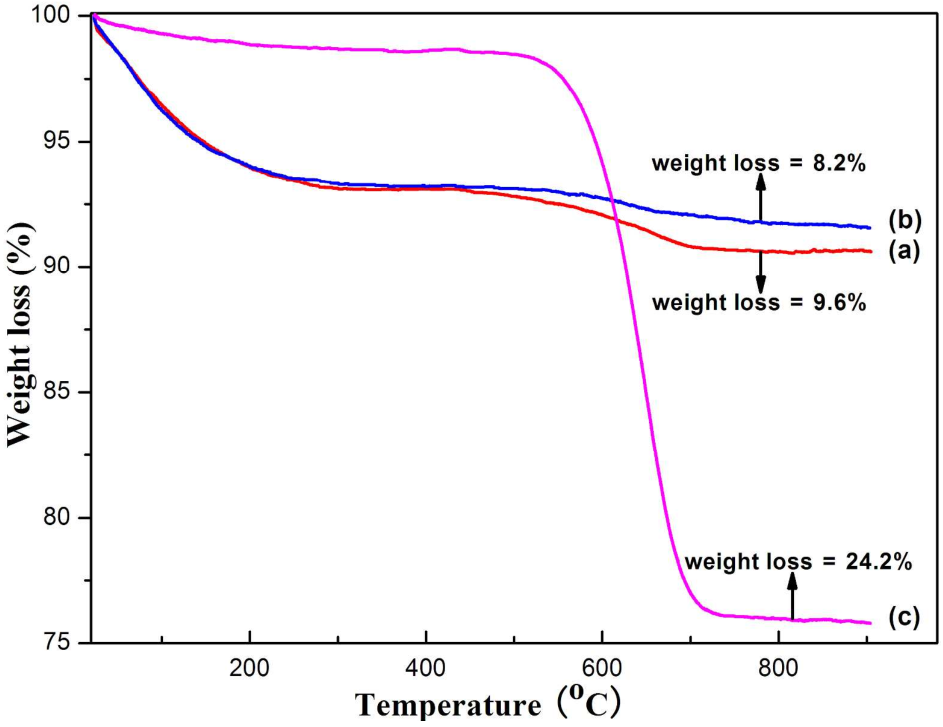
100
95
90
85
80
75
Weight loss (%)
200
400
600
800
Temperature (°C)
weight loss = 8.2%
(b)
(a)
weight loss = 9.6%
weight loss = 24.2%
(c)

Figure 10

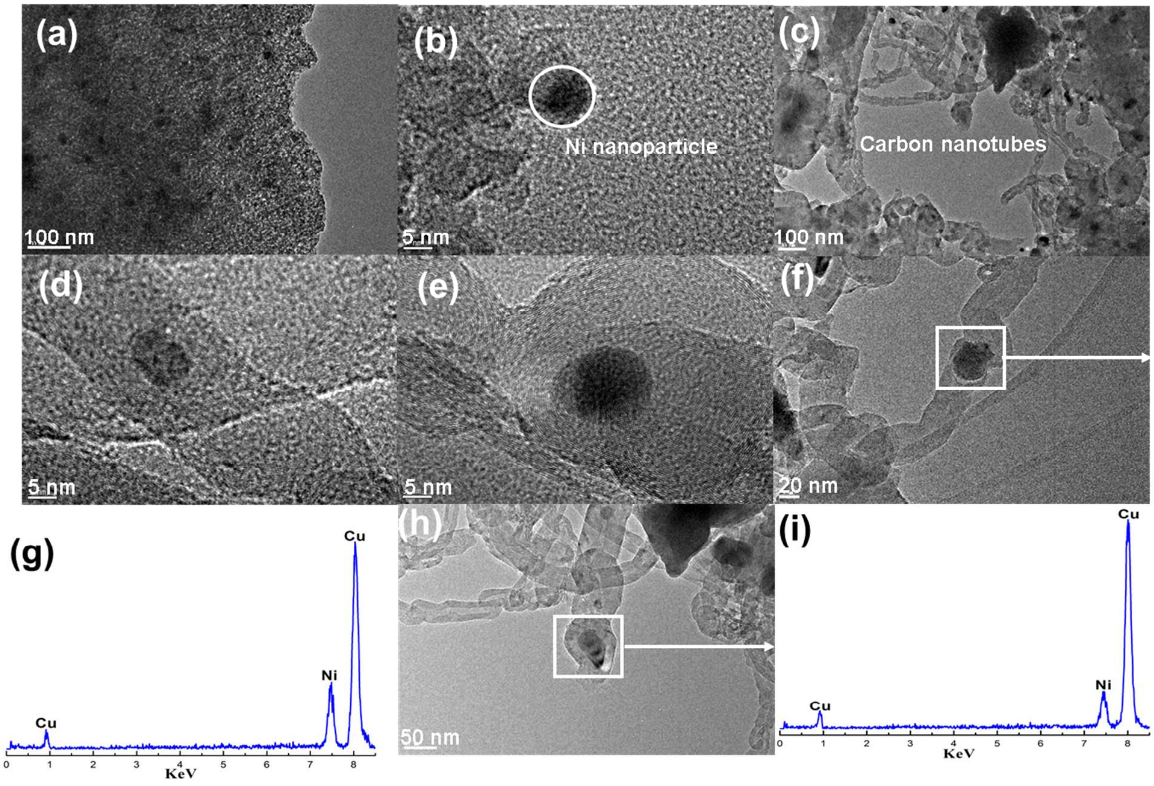
(a)
100 nm
(b)
Ni nanoparticle
5 nm
(c)
Carbon nanotubes
100 nm
(d)
5 nm
(e)
5 nm
(f)
20 nm
(g)
Cu
Ni
Cu
0 1 2 3 4 5 6 7 8
KeV
(h)
50 nm
(i)
Cu
Ni
Cu
0 1 2 3 4 5 6 7 8
KeV

Figure 11